Kayoung Park
Department of Chemical Engineering,
Faculty of Engineering,
Kyushu University,
Nishi-ku, Fukuoka 819-0395, Japan
e-mail: kpark@chem-eng.kyushu-u.ac.jp

Yuting Wei
Department of Chemical Engineering,
Faculty of Engineering,
Kyushu University,
Nishi-ku, Fukuoka 819-0395, Japan
e-mail: weiyuting@kyudai.jp

Magnus So
Department of Chemical Engineering,
Faculty of Engineering,
Kyushu University,
Nishi-ku, Fukuoka 819-0395, Japan
e-mail: magnus_so@chem-eng.kyushu-u.ac.jp

Tae Hyoung Noh
Department of Chemical Engineering,
Faculty of Engineering,
Kyushu University,
Nishi-ku, Fukuoka 819-0395, Japan
e-mail: yarn4828@kyudai.jp

Naoki Kimura
Department of Chemical Engineering,
Faculty of Engineering,
Kyushu University,
Nishi-ku, Fukuoka 819-0395, Japan
e-mail: nkimura@chem-eng.kyushu-u.ac.jp

Yoshifumi Tsuge
Department of Chemical Engineering,
Faculty of Engineering,
Kyushu University,
Nishi-ku, Fukuoka 819-0395, Japan
e-mail: tsuge@chem-eng.kyushu-u.ac.jp

Gen Inoue[1]
Department of Chemical Engineering,
Faculty of Engineering,
Kyushu University,
Nishi-ku, Fukuoka 819-0395, Japan
e-mail: ginoue@chem-eng.kyushu-u.ac.jp

Influence of Surface Structure on Performance of Inkjet Printed Cathode Catalyst Layers for Polymer Electrolyte Fuel Cells

The structure of the cathode catalyst layer (CCL) is critically important for improving the performance, durability, and stability of polymer electrolyte fuel cells (PEFCs). In this study, we designed CCLs with a three-dimensional (3D) structure that could increase the surface area of the CCLs to decrease their oxygen transfer resistance. The CCLs were fabricated using an inkjet printing method, and the electrochemical performance of the CCLs in a membrane electrode assembly was evaluated using an actual cell. The results showed that at high Pt loadings, the performance of the CCL with the 3D structure was superior to that of the flat structure. In particular, at a high current density, which is related to mass transport resistance, the two structures exhibited a significant difference in performance. At a Pt loading of 0.3 mg/cm^2, the CCL with the 3D structure showed the highest maximum power density among all the CCLs investigated in this study. This indicates that the 3D structure decreases the oxygen transfer resistance of the CCL. Overall, the 3D structure provided improved morphological and microstructural characteristics to the CCL for fuel cell applications. [DOI: 10.1115/1.4052629]

Keywords: electrochemical engineering, fuel cells

1 Introduction

Owing to their high energy efficiency, simplicity, low operation temperature (20–100 °C), emission-free nature (CO, CO_2, and NO_x), and quick start and shutdown features, polymer electrolyte fuel cells (PEFCs) are considered as promising power sources for next-generation transportation and electronic devices, such as fuel cell vehicles, that operate on hydrogen energy. PEFCs have been extensively investigated over the past few decades for their application as automotive power sources. However, the applications of PEFCs remain limited because of their high cost, insufficient performance, and durability [1,2]. As the oxygen reduction reaction (ORR) at the cathode is the dominant reaction in PEFCs, oxygen, protons, and electrons must be transferred smoothly to the porous cathode catalyst layer (CCL), as shown in Fig. 1(*a*). Protons are delivered through an ionomer network, such as Nafion, and electrons move through a conductive material, such as carbon black. In addition, oxygen passes through the CCL via gas pores, dissolves into the ionomer, and moves through it to the Pt surface where the ORR occurs. Oxygen transfer is the dominant factor affecting the limiting current density because of the occurrence of resistance in both the gas and ionomer phases; therefore, it is important to increase the oxygen transfer from the gas channel to the Pt surface through various porous media and components [3–6].

To investigate and optimize mass transport in CCLs, various studies focusing on ionomer films (where oxygen diffusion occurs), CCL structures, Pt dispersity, porous carbon, and humidity, which can affect the oxygen transfer resistance [7–13] of CCLs,

[1]Corresponding author.

Manuscript received July 19, 2021; final manuscript received September 13, 2021; published online October 20, 2021. Assoc. Editor: Lei Zhang.

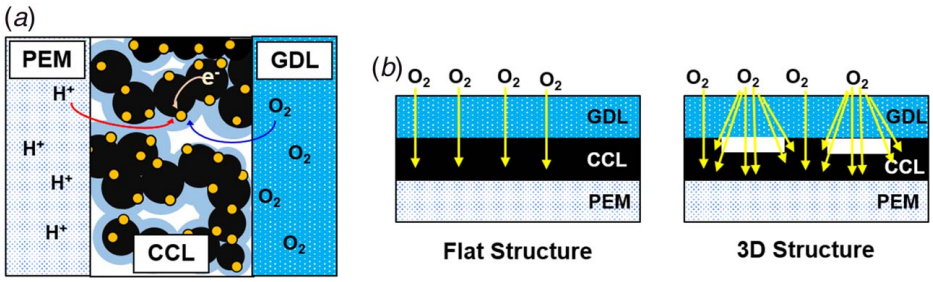

Fig. 1 Schematic of (*a*) the cathode side and (*b*) the two CCL structural designs

have been conducted. For example, Inoue et al. [8] investigated the relationship between the oxygen transfer resistance of porous components and their three-dimensional (3D) structures. They performed numerical simulations to model the properties of oxygen transport. They found that the relative diffusion coefficient of the CCL, which is the ratio of its effective diffusion coefficient to the bulk molecular diffusion coefficient, was an order of magnitude lower than those of the gas diffusion layer (GDL) and microporous layer. Moreover, an equation related to the relative diffusion coefficient was obtained as a function of the porosity. In addition, various methods have been used to investigate the oxygen mass transport resistance in PEFCs. O'Neil et al. [14] suggested techniques to differentiate between the mass transport resistance within the CCL and within the GDL for PEFCs. Oxygen gain is the difference in performance under oxygen-depleted and oxygen-rich cathode fuel streams and represents the degree of oxygen mass transport resistance within the PEFC. For mass transfer resistance within the CCL, the oxygen gain values were limited to a finite range of values. In contrast, for the mass transfer resistance within the GDL, the oxygen gain was not restricted to a finite range of values. These studies identified the key factors that can reduce oxygen transfer resistance of CCLs for PEFCs, thus improving cell performance.

In order to optimize the CCLs considering their mass transport properties, the fabrication process is important because the CCL morphology depends on factors such as the composition of the catalyst ink and the fabrication method. Catalyst ink, which is composed of carbon-supported Pt catalysts, solvents, and an ionomer, is used for the fabrication of CCLs, and the ink solvents can influence the ionomer distribution within the CCL, affecting the cell performance [15–17]. Moreover, various methods, such as doctor blade, brush painting, spraying, and inkjet printing, have been used to fabricate CCLs [18–22]. In particular, inkjet printing is considered as an economical and easy scale-up technology for microscale patterning and fabrication for a variety of applications because it allows for the patterning of various inks. In addition, it can reduce the processing time and cost during the manufacturing process [23]. This method can also be readily applied to studies on ink composition. In particular, for fuel cell applications, inkjet printing resolves many of the problems associated with previously reported catalyst deposition methods by allowing for uniform catalyst ink distribution on the surface of the Nafion membrane and by loading a very small amount of the catalyst [24].

Furthermore, inkjet printing technologies have been widely used in electrochemical energy applications for the fabrication of 3D structures [25–27]. In particular, 3D printing technologies have been utilized for manufacturing supercapacitors and lithium-ion batteries. Zhu et al. [28] reported the fabrication of 3D periodic graphene composite aerogel microlattices for supercapacitor applications using the direct-ink writing process, a 3D printing technique. The 3D-printed graphene composite aerogel electrodes were light-weight and exhibited high conductivity and excellent electrochemical properties. Liu et al. [29] fabricated electrodes for lithium-ion batteries via low-temperature direct writing-based 3D printing (LTDW) for comparison with the roller coating process. The LTDW-fabricated electrodes showed the best performance with an optimal specific capacity at high solid contents. Owing to its wide range of applications, 3D printing technology can be used to fabricate CCLs for high-performance PEFCs.

In this study, we fabricated CCLs with 3D structures via an inkjet printing method used in a previous study to improve the performance of PEFCs [24]. In addition, a CCL with a flat structure was fabricated for comparison. As shown in Fig. 1(*b*), the 3D structure of the CCL increased its surface area for contact with oxygen, leading to a decrease in the oxygen diffusion resistance. We analyzed the morphologies and electrochemical performances of both structures.

2 Theoretical Estimation

Simple theoretical equations were used in this study to understand the effect of the 3D structure on the CCL properties. The Butler-Volmer equation r_{O_2} was converted into a first-order reaction with the assumption that the reaction was isothermal and limited by the oxygen diffusion in the CCL as follows [7]:

$$r_{O_2} = a_{Pt}^{eff}\frac{i_{Pt}}{4F} = a_{Pt}^{eff}\frac{1}{4F}\frac{i_0^{ref}}{C_{O_2}^{ref}}\exp\left(\frac{-n\alpha_c F}{RT}\eta_{local}\right)\frac{RT}{H}C_{O_2}^{pore} \quad (1)$$

where i_{Pt} is the current density on the Pt surface, F is Faraday's constant, i_0^{ref} is the exchange current density, $C_{O_2}^{ref}$ is the reference oxygen concentration, a_{Pt}^{eff} is the effective Pt surface area per local volume, n is the number of electrons, α_c is the charge-transfer coefficient, R is the gas constant, T is temperature, η_{local} is the local overvoltage, H is Henry's coefficient, and $C_{O_2}^{pore}$ is the oxygen concentration in the local pore space

$$k_{O_2} = \frac{1}{4F}\frac{i_0^{ref}}{C_{O_2}^{ref}}a_{Pt}^{eff}\exp\left(\frac{-n\alpha_c F}{RT}\eta_{local}\right)\frac{RT}{H} \quad (2)$$

where k_{O_2} is the first-order reaction coefficient of oxygen.

In addition, the diffusion length and Thiele modulus were introduced to consider the effect of the CCL structure. The Thiele modulus is the ratio of the kinetic reaction rate to the diffusion rate of the reactant. When the Thiele modulus is small, diffusion limitations are negligible, and the reaction rate is kinetically controlled. In contrast, when the Thiele modulus is large, kinetic limitations are negligible, and the reaction rate is controlled by diffusion [14]. Herein, the Thiele modulus was used to estimate the effectiveness factor of the CCLs.

The reactant diffusion lengths of the CCLs, L_D, were calculated using the following equation:

$$L_D = \frac{w_s}{w_s + h_s}h_{CL} \quad (3)$$

where w_s is the gap width, h_s is the gap height, and h_{CL} is the thickness of the catalyst layer, as illustrated in Fig. 2(*a*). The Thiele

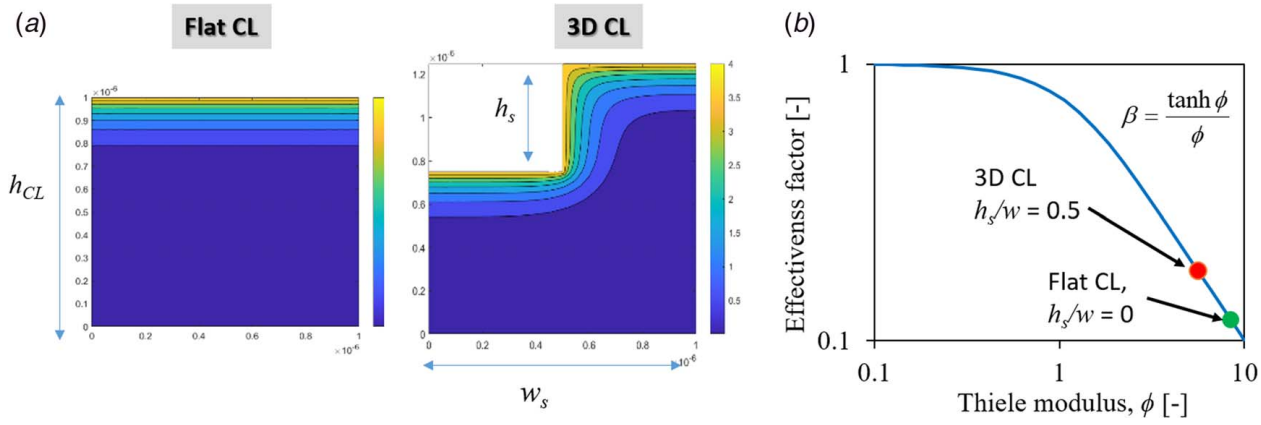

Fig. 2 Calculation of (*a*) the diffusion length and (*b*) the relationship between the effectiveness factor and the Thiele modulus of the CCLs with the two structures

modulus is a dimensionless quantity and can be expressed using k_{O_2} and L_D as follows:

$$\varnothing = L_D\sqrt{\frac{k_{O_2}}{D_{O_2}^{eff}}} \tag{4}$$

The effective oxygen diffusion coefficient $D_{O_2}^{eff}$ was calculated using the following relation:

$$D_{O_2}^{eff} = D_{O_2}\varepsilon^6 \tag{5}$$

where D_{O_2} is bulk oxygen diffusion coefficient. The sixth power of porosity is a fitting parameter that includes the combined effect of tortuosity and the Knudsen diffusion effect and has been confirmed by conducting experiments on the CCLs [8].

As mentioned earlier, the Thiele modulus was used to estimate the effectiveness factor of the CCLs. An effectiveness factor in the range of 0–1 for isothermal conditions indicates the importance of diffusion and kinetic limitations and can also be considered as the amount of reactants that penetrate the CCL [14]. The effectiveness factor is expressed as follows:

$$\beta = \frac{\tanh\varnothing}{\varnothing} \tag{6}$$

and when the resistance to mass transport within a CCL is the rate-limiting factor ($\varnothing$ is large) [14]:

$$\beta \approx \frac{1}{\varnothing} \tag{7}$$

If diffusion is the rate-limiting step, the limiting current density i_{lim}, which is obtained from flux to the CCL, can be derived as follows:

$$i_{lim} = \frac{h_{CL}}{L_D}4FC_{channel}\sqrt{kD_{O_2}^{eff}} \tag{8}$$

where $C_{channel}$ is the gas channel oxygen concentration.

Parameters used for theoretical estimations are listed in Table 1.

Figure 2 shows the diffusion lengths of the CCLs with various structures and the relationship between the Thiele modulus and the effectiveness factors of the CCLs. In the oxygen diffusion-limited range, the CCL with the 3D structure showed better performance than the CCL with flat structure. Thus, the effect of the 3D structure could be estimated using the theoretical method, and experiments were conducted to verify this result.

Table 1 List of parameters for theoretical estimation

Symbol	Parameter	Value	Unit
F	Faraday's constant	8.6	mol/m^3
H	Henry's coefficient	0.3125	–
R	Gas constant	8.314	J/(K · mol)
T	Temperature	80	°C
α_c	Charge-transfer coefficient	0.5	–
η_{local}	Local overvoltage	0–1.2	V
$C_{O_2}^{ref}$	Reference oxygen concentration	8.6	mol/m^3
$C_{O_2}^{pore}$	Oxygen concentration in the local pore space	7.14	mol/m^3

3 Experimental

3.1 Preparation of Cathode Catalyst Ink and Membrane Electrode Assembly Fabrication. A carbon-supported Pt catalyst (TEC10V50E; Pt loading: 46.8%), purchased from Tanaka Kikinzoku Kogyo, was mixed with distilled water and 1-Propanol (NPA). The ratio of water to NPA was 1:80. The slurry was dispersed using an ultrasonic homogenizer for 20 min after the addition of the ionomer (Nafion solution 20 mass%, Sigma-Aldrich). The ionomer-to-carbon (I/C) mass ratio was adjusted to 0.25. Cathode inks were used for CCL fabrication. First, a Nafion film (NR-211, Chemours) was assembled with an anode CL (TEC10E30E, Tanaka Kikinzoku Kogyo, Tokyo, Japan) containing Pt (0.21 mg/cm^2 and compressed using hot pressing at 413 K and 6 MPa for 4 min. The cathode ink was then printed directly onto the Nafion film using the inkjet printing method. Figure 3(*a*) shows real inkjet printing images and Fig. 3(*b*) shows patterning of the CCL structures. The ink dropped through the head onto the Nafion membrane to form a CL. In this study, CCLs with two surface structures were fabricated: flat and 3D structures printed with varying ink patterns, as shown in Fig. 3(*b*). First, to make the patterns of each structure, a drop of catalyst ink dried on the Nafion membrane was observed to obtain information about the diameter, radius, width, and thickness. Next, a pattern made with the radius length intervals of a drop of ink was applied to fabricate the flat structure. The catalyst ink was dropped continuously until the deposition of one layer was completed and then dried to avoid shape formation on the surface of the CCL. On the other hand, for the 3D structures, patterns were created by the overlapping outer and inner diameters with varying thicknesses at equal intervals based on information obtained from the ink drops. However, because the continuous dropping of ink did not form a shape, it was immediately dried after printing a drop, in order for the dried ink droplets to overlap. The Pt loading of the CCLs with the two

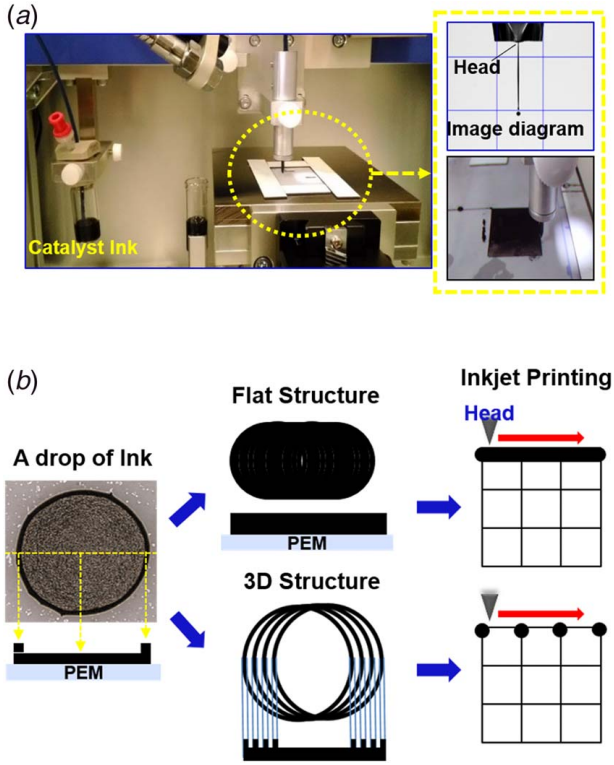

Fig. 3 Real images of (*a*) inkjet printing and (*b*) patterning of the CCL structures

different structures varied from 0.2 to 0.5 mg/cm^2. The structures and Pt loadings of the samples are listed in Table 2. The fabricated membrane electrode assemblies (MEAs) with an active area of 1 cm^2 were composed of the anode and cathode CLs on either side of the Nafion film. Gas diffusion layers (Sigracet25BC, SGL Carbon) containing 5% PTFE with a thickness of 235 μm were used on both the anode and cathode sides.

3.2 Electrochemical Measurements and Characterization. Electrochemical measurements were performed using a single cell (JARI, serpentine: 1 mm width, 1 mm depth). The following aging conditions were used: pure H_2 gas and 21% O_2 with pure N_2 were humidified and supplied to the anode and cathode, respectively. The aging step was performed while cycling the potential between the open circuit voltage and 0.3 V for 30 s until the current reached a constant value at 0.3 V. The polarization curves of the CCLs were measured over the potential range of 0.9–0.2 V at a potential drop rate of 0.1 V. Each potential was maintained for 5 min until the current stabilized, and electrochemical impedance spectroscopy (EIS) measurements were conducted over a frequency range of 100 kHz–0.2 Hz. The measurement temperature was 80 °C and the relative humidity was 100%. The gas flow rates were 250 and 500 ml/min at the anode and cathode, respectively.

Table 2 Sample information

Sample	Structure	Pt loading (mg$_{Pt}$/cm^2)	h_{CL} (μm)	h_s (μm)	w_s (μm)
Flat_Pt0.2	Flat	0.2	4.8	–	–
Flat_Pt0.3	Flat	0.3	7.6	–	–
Flat_Pt0.5	Flat	0.5	11.8	–	–
3D_Pt0.2	3D	0.2	5.8	2.0	16
3D_Pt0.3	3D	0.3	9.0	2.8	16
3D_Pt0.5	3D	0.5	14.8	6.0	16

The thickness of a drop of ink dried on the Nafion film was determined, and the morphologies of the CCLs with flat and 3D structures were examined using a laser confocal microscope (OLS-4500, Olympus, Japan).

4 Results and Discussion

4.1 Structural Characterization. To obtain basic information regarding the patterning of the 3D structures, the morphologies and lengths of the ink droplet layers printed on the Nafion film were measured using a laser microscope. Figures 4(*a*) and 4(*b*) show the images of the first and fifth printed layers on the Nafion film, respectively. The edges of the first layer were darker than the interior. The liquid that evaporated from the edges was replenished by the liquid from the interior, resulting in a coffee ring effect, which led to a drop in coffee dry [30,31]. As the number of layers increased, the concentration of the interior section increased, and that of the edge remained almost the same. This difference in the concentration was caused by the difference in the thickness of the droplet (Fig. 4(*c*)). It was found that with an increase in the number of layers, the thickness of the edge section increased significantly compared with that of the interior part. On the other hand, the ring-like shape of the droplet remained unchanged regardless of the number of layers. Generally, researchers avoid the coffee ring effect in the fabrication of fuel cell catalyst structures because it leads to an uneven surface. In this study, we utilized surface roughness to increase the surface area of the CCLs. For the flat structure, the catalyst ink was dropped continuously until the entire catalyst layer was deposited. In contrast, the ink for the 3D structure was dried immediately after printing each droplet. Owing to the coffee ring effect, a 3D structure with a rough surface was developed. Images of the as-fabricated CCL structures are shown in Figs. 4(*d*) and 4(*e*). The flat structure showed an even surface with a uniform thickness, whereas the 3D structure showed a rough surface, as expected. The structural parameters of the CCLs with the two structures and different Pt loadings are summarized in Table 1. The thickness of the flat structures (Flat_Pt0.2, Flat_Pt0.3, and Flat_Pt0.5) increased with increasing Pt loading. In the case of the 3D structures, the heights and widths of the droplet layers were divided into h_{CL}, h_s, and w_s, as shown in Fig. 4(*e*). With an increase in Pt loading, h_{CL} increased linearly, while w_s remained nearly constant. This confirms the successful fabrication of 3D_Pt0.2, 3D_Pt0.3, and 3D_Pt0.5 3D structures via inkjet patterning.

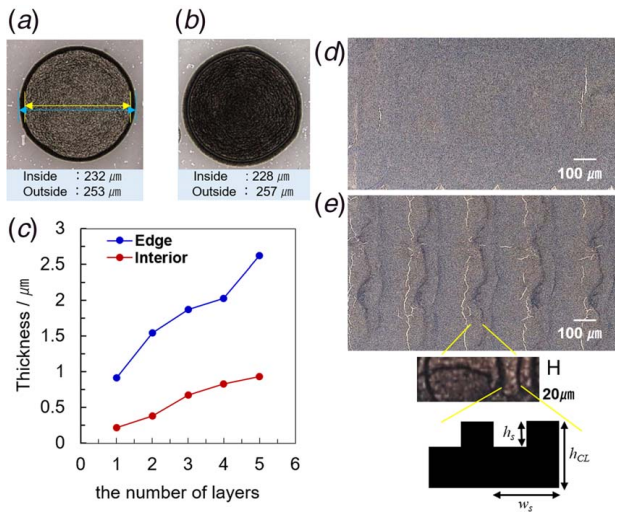

Fig. 4 The images of the (*a*) first and (*b*) fifth printed layers on the Nafion film. (*c*) The thickness of the CCL as a function of the number of layers. Images of the (*d*) flat and (*e*) 3D structures.

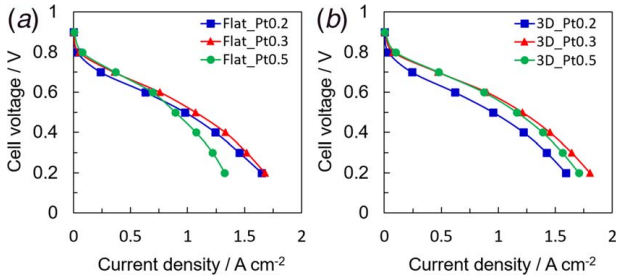

Fig. 5 Polarization curves of the (*a*) flat- and (*b*) 3D-structured CCLs at Pt loadings of 0.2, 0.3, and 0.5 mg/cm^2

4.2 Electrochemical Analysis of the Two Structures. Figure 5 shows the polarization curves of the MEAs with flat and 3D structures and varying Pt loadings. In the case of the flat structures (Fig. 5(*a*)), the performance of Flat_Pt0.3 was slightly better than that of Flat_Pt0.2. However, the performance of Flat_Pt0.5 began to deteriorate at 0.6 A/cm^2 and dropped sharply at high current densities. This indicates that at high current densities, the oxygen diffusion resistance of the CCLs, which was attributed to their mass transport, increased with an increase in Pt loading. On the other hand, the performance of the 3D_Pt0.3 CCL was better than that of 3D_Pt0.2, and the high performance was maintained in 3D_Pt0.5 despite its higher thickness. In other words, with an increase in Pt loading, the 3D structures inhibited the increase in the oxygen diffusion resistance of the CCL. Thus, at a Pt loading of 0.5 mg/cm^2, the CCL with the 3D structure showed a lower reduction rate than that with the flat structure. These results indicate that the surface structure of the CCLs significantly affects their mass transfer.

Figure 6 shows the polarization curves and power densities of the CCLs with various surface structures and Pt loadings. The Flat_Pt0.2 and 3D_Pt0.2 CCLs showed comparable polarization curves and power densities, as shown in Fig. 6(*a*). This indicates that at low Pt loadings, the surface structure did not affect the performance of the CCLs because the thickness of the CCLs was too small; thus, mass transport occurred smoothly on the surface, implying that diffusion becomes less significant. The performance of 3D_Pt0.3 was slightly better than that of Flat_Pt0.3 (Fig. 6(*b*)). The power densities of 3D_Pt0.3 were also higher than those of Flat_Pt0.3 at current densities lower than 1.33 A/cm^2. The effect of the surface structure on the mass transport of the CCLs was observed at Pt loading of 0.3 mg/cm^2. As shown in Fig. 6(*c*), the difference in the performances of the flat- and 3D-structured CCLs was significant at a Pt loading of 0.5 mg/cm^2. In particular, in the higher current density region, the two structures exhibited appreciable differences in performance. In addition, the power densities of both structures exhibited the same tendency. The performances and maximum power densities of the CCLs with the two different structures at varying Pt loadings were analyzed in detail, as shown in Fig. 7. During the oxygen reduction reaction, at a cell voltage of 0.8 (Fig. 7(*a*)), the performances of the CCLs with flat and 3D improved with an increase in Pt loading due to the increase in the number of Pt active sites. This is consistent with previously reported results [32,33]. The reaction of the 3D structure was superior to that of the flat structure. When the cell voltage was 0.2 V for the mass transport region (Fig. 7(*b*)), with an increase in the Pt loading from 0.2 to 0.3 mg/cm^2, the performances of the flat- and 3D-structured CCLs increased by 1.8% and 13%, respectively. However, with an increase in the Pt loading from 0.3 to 0.5 mg/cm^2, the performances of the flat- and 3D-structured CCLs decreased by 21% and 5%, respectively. As mentioned earlier, at a Pt loading of 0.5 mg/cm^2, the CCL performance deteriorated because of the increase in mass transport resistance. However, it should be noted that the degree of deterioration was lower in the case of the 3D structure than for the flat structure. Furthermore, the performance of the 3D structure at a Pt loading of 0.5 mg/cm^2 was comparable with that of the flat structure at a Pt loading of 0.3 mg/cm^2. In other words, unlike the flat structure, the 3D structure enabled effective oxygen transport on the surface, reducing the mass transport resistance of the CCL.

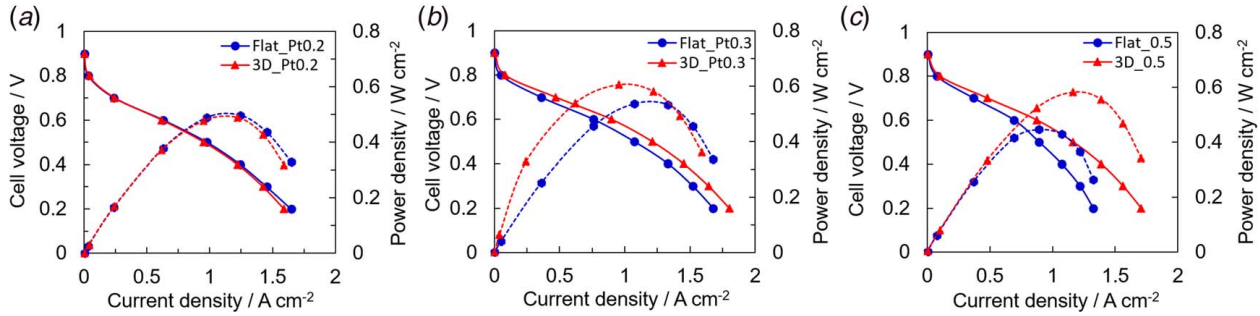

Fig. 6 Polarization curves and power densities of the 3D- and flat-structured CCLs at Pt loadings of (*a*) 0.2, (*b*) 0.3, and (*c*) 0.5 mg/cm^2

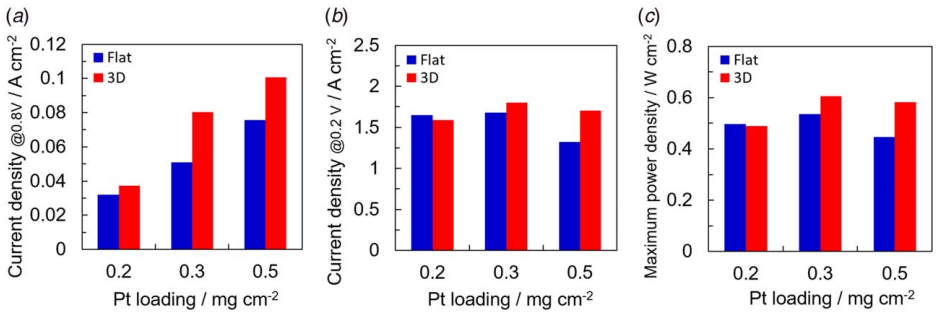

Fig. 7 Performances of the flat and 3D CCLs at (*a*) 0.8 V and (*b*) 0.2 V; and (*c*) maximum power densities of the two structures at various Pt loadings

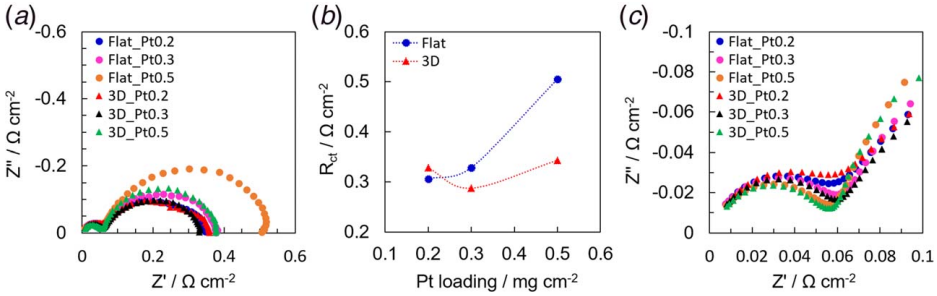

Fig. 8 (*a*) Impedance spectra at 0.6 V of the flat and 3D CCLs and (*b*) charge-transfer resistances of the CCLs at varying Pt loadings. (c) Enlarged impedance spectra of the CCLs over an impedance range of 0–0.1

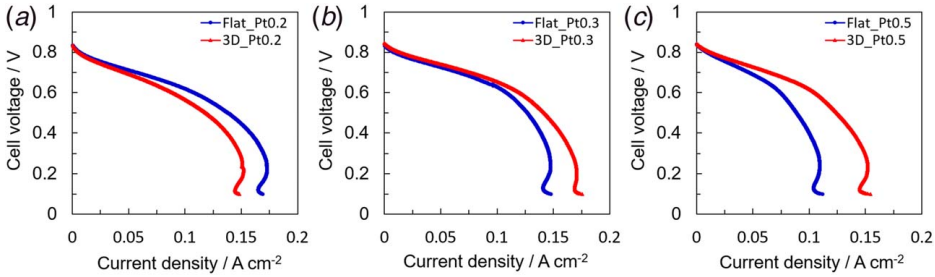

Fig. 9 Limiting current densities of the two structures at Pt loadings of (*a*) 0.2, (*b*) 0.3, and (*c*) 0.5 mg/cm^2

As shown in Fig. 7(*c*), the maximum power density of the CCLs decreased in the following order: 3D_Pt0.3 > 3D_Pt0.5 > Flat_Pt0.3 > Flat_Pt0.2 > 3D_Pt0.2 > Flat_Pt0.5. The 3D_Pt0.3 and 3D_Pt0.5 CCLs outperformed the flat-structured CCLs in terms of the maximum power density, with the highest maximum power density being 0.61 W/cm^2.

Electrochemical impedance spectroscopy was used to quantitatively analyze the relationship between the structure and resistance of the CCLs. Figure 8 shows the impedance spectra of the CCLs with the flat and 3D structures at a range of Pt loadings. The semicircle (on the right) in the Nyquist plots of the CCLs represents the charge-transfer resistance at the cathode. The smaller the diameter of the semicircle was, the lower the CCL resistance was. It was found that the charge-transfer resistance at 0.6 V was the highest for Flat_Pt0.5 and the lowest for 3D_Pt0.3, as shown in Fig. 8(*a*). The charge-transfer resistances of the CCLs changed with the variation in their Pt loading (Fig. 8(*b*)). At a Pt loading of 0.2 mg/cm^2, the charge-transfer resistances of both structures were comparable, resulting in similar cell performances. This indicates that there was no effect of decreasing the oxygen diffusion path, resulting in a reduction in oxygen diffusion resistance because the CCLs were very thin for both the structures at a Pt loading of 0.2 mg/cm^2. At Pt loadings of 0.3 and 0.5 mg/cm^2, the resistances of the 3D-structured CCLs were lower than those of the flat-structured CCLs. Therefore, the higher cell performance of the 3D-structured CCLs can be attributed to their lower charge-transfer resistance. To investigate the effects of other factors, such as proton conductivity, the ohmic resistances of the CCLs were obtained from the high-frequency *X*-intercepts of their Nyquist plots, and Fig. 8(*c*) shows the real impedance (Z') region of the CCLs over the 0–0.1 range. The ohmic resistance of a material represents its resistance to the ionic flow in the electrolyte and to the electronic flow of electronically conductive materials [34]. As shown in Fig. 8(*c*), the ohmic resistances of the samples were dependent on the Pt loading, irrespective of the structure. These results suggest that the conduction in the CCLs was smooth, regardless of their structure because the electrolyte was well-connected. Thus, only the CCL structure affected the performance of the cell.

Figure 9 shows the limiting current densities of the CCLs with the two structures. The limiting current density was measured using 1% oxygen gas. The oxygen-limiting current density was used to quantify the accessibility of oxygen to the catalyst. At a Pt loading of 0.2 mg/cm^2, the CCL with the flat structure showed a slightly lower limiting current density than its 3D-structured counterpart. On the other hand, at higher Pt loadings of 0.3 and 0.5 mg/cm^2, the CCLs with the 3D structure showed higher limiting current densities than those with the flat structure. This result indicates that in the 3D structure, oxygen diffused smoothly to the membrane because of the expansion of the surface area, resulting in increased accessibility to oxygen. In addition, the ratio of the limiting current densities of the flat and 3D structures was evaluated experimentally and theoretically to confirm the effect of the structure. At a Pt loading of 0.5 mg/cm^2, the 3D-structured CCL showed a higher current density (0.154 A/cm^2) than the flat-structured CCL (0.112 A/cm^2). As a result, the ratio of the limiting current density of the 3D structure to that of the flat structure was approximately 1.38. Moreover, theoretical calculations were performed using Eqs. (3) and (8). In Eq. (8), all the variables are constant except for i_{lim} and L_{D}, resulting in the modified equation for the comparison of the flat and 3D structures, as shown below:

$$\frac{i_{\text{lim}}^{\text{3D}}}{i_{\text{lim}}^{\text{Flat}}} = \frac{L_{\text{D}}^{\text{Flat}}}{L_{\text{D}}^{\text{3D}}} \tag{9}$$

where $i_{\text{lim}}^{\text{3D}}$ and $i_{\text{lim}}^{\text{Flat}}$ are the limiting current densities of the 3D and flat structures, respectively. In addition, L_{D}^{3D} and $L_{\text{D}}^{\text{Flat}}$ are the diffusion lengths, which are calculated using the following relations:

$$L_{\text{D}}^{\text{Flat}} = h_{\text{CL}} \tag{10}$$

$$L_{\text{D}}^{\text{3D}} = \frac{h_{CL} w_S}{w_s + h_s} \tag{11}$$

As a result, the ratio of these values is approximately 1.38. In other words, the theoretical and experimental limiting current

density ratios were the same. Thus, the effect of the 3D structure on the performance of the CCL was investigated experimentally and theoretically. The data obtained from the limiting current measurements support the superior performance of the 3D-structured CCLs compared with that of the flat-structured CCLs, as indicated by the I-V curves.

In conclusion, the 3D-structured CCLs exhibited enhanced performances with increasing Pt loading by mitigating the mass transport resistance compared with the flat-structured CCLs. In addition, the 3D-structured CCLs showed a higher mass activity (7.6 A/g_{Pt}) than the flat-structured CCLs (6.3 A/g_{Pt}), calculated at 0.9 V of the polarization curves (Fig. 6), indicating that the 3D structure contributes to Pt utilization. 3D-structured CCLs can be extensively applied not only to Pt, but also to the optimization of CCLs for non-precious metal catalysts with high metal loading.

5 Conclusions

- In this study, we designed CCLs with a 3D structure, thereby, increasing their surface area of the CCLs to decrease their oxygen transfer resistance. CCLs with a flat structure were also designed for comparison. Theoretical calculations predicted that the 3D structure would perform better than the flat structure by comparing the effectiveness factor in the case of limited oxygen diffusion. Thus, these CCLs with the two structures were experimentally fabricated and electrochemically evaluated to validate the prediction. Two types of CCL structures were fabricated using an inkjet printing method using different types of patterning. As a result, flat and 3D CCLs were successfully fabricated, and it was found that the surface of the 3D structure was rough, whereas that of the flat structure was smooth**.**
- The electrochemical performances of the CCLs with the two structures and varying Pt loadings were analyzed. At Pt loadings of 0.3 and 0.5 mg/cm^2, the performances of the 3D structures were superior to those of the flat structures. The maximum power densities of 3D structures with Pt loadings of 0.3 and 0.5 mg/cm^2 were also higher than their flat-structured counterparts, and the highest maximum power density was 0.61 W/cm^2. The 3D structure increased the surface area of the CCL, leading to a decrease in its oxygen transport resistance. The impedance and limiting current density results also support the conclusion that the structure of the CCL affects its performance. Finally, the ratio of the limiting current densities of the two structures was evaluated experimentally and theoretically, and the ratio of these values was the same (approximately 1.38). These results confirmed that the CCL with the 3D-structured CCL was superior to a flat-structured CCL. In the future, we will use computational methods to investigate the effect of the 3D structure on the performance of CCLs under various conditions.

Acknowledgment

This research was supported by Next-Generation Fuel Cell Research Center (NEXT-FC) of Kyushu University, Japan.

Conflict of Interest

There are no conflicts of interest.

Data Availability Statement

The authors attest that all data for this study are included in the paper.

Nomenclature

n = the number of electrons (dimensionless)
F = Faraday's constant (C/mol)
H = Henry's coefficient (dimensionless)
R = gas constant (J/(K · mol))
T = temperature (K)
h_{CL} = thickness of catalyst layer (μm)
h_s = gap height (μm)
i_{lim} = limiting current density (A/cm^2)
i_{Pt} = current density on the Pt surface (A/m^2)
k_{O_2} = first-order reaction coefficient of oxygen (dimensionless)
r_{O_2} = current density per local volume (Butler-Volmer equation) (A/m^3)
w_s = gap width (μm)
$C_{channel}$ = gas channel oxygen concentration (mol/m^3)
D_{O_2} = bulk oxygen diffusion coefficient (m^2/s)
L_D = reactant diffusion lengths of the CCLs (μm)
a_{Pt}^{eff} = effective Pt surface area per local volume (m^2/m^3)
i_{lim}^{3D} = limiting current densities of the 3D structures (A/cm^2)
i_{lim}^{Flat} = limiting current densities of the flat structures (A/cm^2)
i_0^{ref} = exchange current density (A/m^2)
$C_{O_2}^{pore}$ = oxygen concentration in the local pore space (mol/m^3)
$C_{O_2}^{ref}$ = reference oxygen concentration (mol/m^3)
$D_{O_2}^{eff}$ = effective oxygen diffusion coefficient (m^2/s)
L_D^{3D} = diffusion lengths of 3D structures (μm)
L_D^{Flat} = diffusion lengths of flat structures (μm)
α_c = charge-transfer coefficient (dimensionless)
β = effectiveness factor (dimensionless)
ε = porosity (dimensionless)
η_{local} = local overvoltage (V)
$\varnothing$ = Thiele modulus (dimensionless)

References

[1] Inoue, G., 2016, "Secondary Batteries and Fuel Cell Systems for Next-Generation Vehicles," *Energy Technology Roadmaps of Japan*, Y. Kato, M. Koyama, Y. Fukushima, and T. Nakagaki, eds., Springer Japan, Tokyo, pp. 537–547.
[2] Debe, M. K., 2012, "Electrocatalyst Approaches and Challenges for Automotive Fuel Cells," Nature, **486**(7401), pp. 43–51.
[3] Yoon, W., and Weber, A. Z., 2011, "Modeling Low-Platinum-Loading Effects in Fuel-Cell Catalyst Layers," J. Electrochem. Soc., **158**(8), p. B1007.
[4] Wilson, A., Kleen, G., and Papageorgopoulos, D., 2017, "DOE Hydrogen and Fuel Cells Program Record," Fuel Cell System Cost—2017.
[5] Liu, W., Suzuki, T., Mao, H., and Schmiedel, T., 2013, "Development of Thin, Reinforced PEMFC Membranes Through Understanding of Structure-Property-Performance Relationships," ECS Trans., **50**(2), pp. 51–64.
[6] Darling, R. M., 2018, "A Hierarchical Model for Oxygen Transport in Agglomerates in the Cathode Catalyst Layer of a Polymer-Electrolyte Fuel Cell," J. Electrochem. Soc., **165**(9), pp. F571–F580.
[7] So, M., Park, K., Tsuge, Y., and Inoue, G., 2020, "A Particle Based Ionomer Attachment Model for a Fuel Cell Catalyst Layer," J. Electrochem. Soc., **167**(1), p. 013544.
[8] Inoue, G., Yokoyama, K., Ooyama, J., Terao, T., Tokunaga, T., Kubo, N., and Kawase, M., 2016, "Theoretical Examination of Effective Oxygen Diffusion Coefficient and Electrical Conductivity of Polymer Electrolyte Fuel Cell Porous Components," J. Power Sources, **327**, pp. 610–621.
[9] Sambandam, S., Parrondo, J., and Ramani, V., 2013, "Estimation of Electrode Ionomer Oxygen Permeability and Ionomer-Phase Oxygen Transport Resistance in Polymer Electrolyte Fuel Cells," Phys. Chem. Chem. Phys., **15**(36), pp. 14994–15002.
[10] Sun, X., Yu, H., Zhou, L., Gao, X., Zeng, Y., Yao, D., He, L., and Shao, Z., 2020, "Influence of Platinum Dispersity on Oxygen Transport Resistance and Performance in PEMFC," Electrochim. Acta, **332**, p. 135474.
[11] Cetinbas, F. C., Ahluwalia, R. K., Kariuki, N. N., De Andrade, V., and Myers, D. J., 2020, "Effects of Porous Carbon Morphology, Agglomerate Structure and Relative Humidity on Local Oxygen Transport Resistance," J. Electrochem. Soc., **167**(1), p. 013508.
[12] Inoue, G., Ohnishi, T., So, M., Park, K., Ono, M., and Tsuge, Y., 2019, "Simulation of Carbon Black Aggregate and Evaluation of Ionomer Structure on Carbon in Catalyst Layer of Polymer Electrolyte Fuel Cell," J. Power Sources, **439**, p. 227060.
[13] So, M., Park, K., Ohnishi, T., Ono, M., Tsuge, Y., and Inoue, G., 2019, "A Discrete Particle Packing Model for the Formation of a Catalyst Layer in Polymer Electrolyte Fuel Cells," Int. J. Hydrogen Energy, **44**(60), pp. 32170–32183.
[14] O'Neil, K., Meyers, J. P., Darling, R. M., and Perry, M. L., 2012, "Oxygen Gain Analysis for Proton Exchange Membrane Fuel Cells," Int. J. Hydrogen Energy, **37**(1), pp. 373–382.

[15] Fernández, R., Ferreira-Aparicio, P., and Daza, L., 2005, "PEMFC Electrode Preparation: Influence of the Solvent Composition and Evaporation Rate on the Catalytic Layer Microstructure," J. Power Sources, **151**(1–2), pp. 18–24.
[16] Ngo, T. T., Yu, T. L., and Lin, H. L., 2013, "Influence of the Composition of Isopropyl Alcohol/Water Mixture Solvents in Catalyst Ink Solutions on Proton Exchange Membrane Fuel Cell Performance," J. Power Sources, **225**, pp. 293–303.
[17] So, M., Ohnishi, T., Park, K., Ono, M., Tsuge, Y., and Inoue, G., 2019, "The Effect of Solvent and Ionomer on Agglomeration in Fuel Cell Catalyst Inks: Simulation by the Discrete Element Method," Int. J. Hydrogen Energy, **44**(54), pp. 28984–28995.
[18] Suzuki, T., Tsushima, S., and Hirai, S., 2013, "Fabrication and Performance Evaluation of Structurally-Controlled PEMFC Catalyst Layers by Blending Platinum-Supported and Stand-Alone Carbon Black," J. Power Sources, **233**, pp. 269–276.
[19] Mao, Q., Sun, G., Wang, S., Sun, H., Wang, G., Gao, Y., Ye, A., Tian, Y., and Xin, Q., 2007, "Comparative Studies of Configurations and Preparation Methods for Direct Methanol Fuel Cell Electrodes," Electrochim. Acta, **52**(24), pp. 6763–6770.
[20] Kim, K.-H., Lee, K.-Y., Kim, H.-J., Cho, E., Lee, S.-Y., Lim, T.-H., Yoon, S. P., Hwang, I. C., and Jang, J. H., 2010, "The Effects of Nafion® Ionomer Content in PEMFC MEAs Prepared by a Catalyst-Coated Membrane (CCM) Spraying Method," Int. J. Hydrogen Energy, **35**(5), pp. 2119–2126.
[21] Chaparro, A. M., Gallardo, B., Folgado, M. A., Martín, A. J., and Daza, L., 2009, "PEMFC Electrode Preparation by Electrospray: Optimization of Catalyst Load and Ionomer Content," Catal. Today, **143**(3–4), pp. 237–241.
[22] Wang, Z., and Nagao, Y., 2014, "Effects of Nafion Impregnation Using Inkjet Printing for Membrane Electrode Assemblies in Polymer Electrolyte Membrane Fuel Cells," Electrochim. Acta, **129**, pp. 343–347.
[23] Shukla, S., Domican, K., Karan, K., Bhattacharjee, S., and Secanell, M., 2015, "Analysis of Low Platinum Loading Thin Polymer Electrolyte Fuel Cell Electrodes Prepared by Inkjet Printing," Electrochim. Acta, **156**, pp. 289–300.
[24] Park, K., Ohnishi, T., Goto, M., So, M., Takenaka, S., Tsuge, Y., and Inoue, G., 2019, "Improvement of Cell Performance in Catalyst Layers With Silica-Coated Pt/Carbon Catalysts for Polymer Electrolyte Fuel Cells," Int. J. Hydrogen Energy, **45**(3), pp. 1867–1877.
[25] Yu, W., Zhou, H., Li, B. Q., and Ding, S., 2017, "3D Printing of Carbon Nanotubes-Based Microsupercapacitors," ACS Appl. Mater. Interfaces, **9**(5), pp. 4597–4604.
[26] Sun, K., Wei, T. S., Ahn, B. Y., Seo, J. Y., Dillon, S. J., and Lewis, J. A., 2013, "3D Printing of Interdigitated Li-Ion Microbattery Architectures," Adv. Mater., **25**(33), pp. 4539–4543.
[27] Gao, T., Zhou, Z., Yu, J., Zhao, J., Wang, G., Cao, D., Ding, B., and Li, Y., 2019, "3D Printing of Tunable Energy Storage Devices With Both High Areal and Volumetric Energy Densities," Adv. Energy Mater., **9**(8), pp. 1–10.
[28] Zhu, C., Liu, T., Qian, F., Han, T. Y. J., Duoss, E. B., Kuntz, J. D., Spadaccini, C. M., Worsley, M. A., and Li, Y., 2016, "Supercapacitors Based on Three-Dimensional Hierarchical Graphene Aerogels With Periodic Macropores," Nano Lett., **16**(6), pp. 3448–3456.
[29] Liu, C., Xu, F., Cheng, X., Tong, J., Liu, Y., Chen, Z., Lao, C., and Ma, J., 2019, "Comparative Study on the Electrochemical Performance of $LiFePO_4$ Cathodes Fabricated by Low Temperature 3D Printing, Direct Ink Writing and Conventional Roller Coating Process," Ceram. Int., **45**(11), pp. 14188–14197.
[30] Yunker, P. J., Still, T., Lohr, M. A., and Yodh, A. G., 2011, "Suppression of the Coffee-Ring Effect by Shape-Dependent Capillary Interactions," Nature, **476**(7360), pp. 308–311.
[31] Choi, S., Stassi, S., Pisano, A. P., and Zohdi, T. I., 2010, "Coffee-Ring Effect-Based Three Dimensional Patterning of Micro/Nanoparticle Assembly With a Single Droplet," Langmuir, **26**(14), pp. 11690–11698.
[32] Sassin, M. B., Garsany, Y., Atkinson, R. W., Hjelm, R. M. E., and Swider-Lyons, K. E., 2019, "Understanding the Interplay Between Cathode Catalyst Layer Porosity and Thickness on Transport Limitations En Route to High-Performance PEMFCs," Int. J. Hydrogen Energy, **44**(31), pp. 16944–16955.
[33] Owejan, J. P., Owejan, J. E., and Gu, W., 2013, "Impact of Platinum Loading and Catalyst Layer Structure on PEMFC Performance," J. Electrochem. Soc., **160**(8), pp. F824–F833.
[34] Bezerra, C. A. G., Deiner, L. J., and Tremiliosi-Filho, G., 2020, "Inkjet Printed Double-Layered Cathodes for PEM Fuel Cells," J. Electrochem. Soc., **167**(12), p. 124503.